Aerosol effect on the distribution of solar radiation over the clear-sky global oceans derived from four years of MODIS retrievals

L. A. Remer, Y. J. Kaufman

**Atmospheric
Chemistry
and Physics
Discussions**

ACPD

5, 5007–5038, 2005

Aerosol effect on
solar radiation from
MODIS

L. A. Remer and
Y. J. Kaufman

Title Page

Abstract   Introduction

Conclusions   References

Tables   Figures

◄   ►

◄   ►

Back   Close

Full Screen / Esc

Print Version

Interactive Discussion

EGU

Aerosol effect on the distribution of solar radiation over the clear-sky global oceans derived from four years of MODIS retrievals

L. A. Remer and Y. J. Kaufman

Laboratory for Atmospheres, NASA/Goddard Space Flight Center, Greenbelt MD 20771, USA

Correspondence to: L. A. Remer (Lorraine.A.Remer@nasa.gov)

Aerosol effect on solar radiation from MODIS

L. A. Remer and
Y. J. Kaufman

Abstract

A four year record of MODIS spaceborne data provides a new measurement tool to assess the aerosol direct radiative effect at the top of the atmosphere. MODIS derives the aerosol optical thickness and microphysical properties from the scattered sunlight at 0.55–2.1 μm. The monthly MODIS data used here are accumulated measurements across a wide range of view and scattering angles and represent the aerosol's spectrally resolved angular properties. We use these data consistently to compute with estimated accuracy of $\pm 0.3\,\text{Wm}^{-2}$ the reflected sunlight by the aerosol over global oceans in cloud free conditions. The MODIS high spatial resolution (0.5 km) allows observation of the aerosol impact between clouds that can be missed by other sensors with larger footprints. We found that over the clear-sky global ocean the aerosol reflected $5.0 \pm 0.3\,\text{Wm}^{-2}$ with an average radiative efficiency of $46 \pm 2\,\text{Wm}^{-2}$ per unit optical thickness. The seasonal and regional distribution of the aerosol radiative effects are discussed. The analysis adds a new measurement perspective to a climate change problem dominated so far by models.

1. Introduction

Traditionally, chemical transport and general circulation models enjoyed a monopoly on estimating the role of aerosols in the Earth's climate. Model results form the basis of almost every previous estimate of the aerosol effect on climate (IPCC, 2001). Observations of aerosols from ground-based, airborne or satellite instruments are used only to validate these models. The prevailing strategy dictates that measurements improve models, and then models, not measurements, answer climate questions. However, there is a wide range of discrepancy in model results because of the many inherent assumptions involved in modeling the aerosol effect on climate. Models must properly estimate the source terms of the many aerosol species, properly model the aerosol sink terms, and simulate the transport. Even if the model properly simulates the global

distribution of aerosol concentration, assumptions have to be made of the aerosol optical properties in order to convert mass concentrations to the radiative fluxes. Because of the complexity of the problem, it is no wonder that the uncertainties in estimating aerosol effects on climate are growing, rather than shrinking.

⁵   To narrow the uncertainties associated with estimating aerosol effects on climate, the time has come to include measurement-based estimates of aerosol radiative effects and forcing. With the launch of EOS-Terra carrying the MODerate resolution Imaging Spectroradiometer (MODIS), Multi-angle Imaging Spectro-Radiometer (MISR) and Clouds and Radiant Energy System (CERES), we are suddenly "data rich". These in-
¹⁰ struments, along with subsequent instruments on EOS-Aqua, EOS-Aura, ICESat, and Parasol, are designed specifically to observe aerosols and the Earth's radiation budget. They provide global information in a way that previous ground-based or airborne instruments could not, and they provide quantitative information about aerosol that is not only more accurate than our heritage instruments, but also more complete in terms
¹⁵ of aerosol characterization. With these increased capabilities, aerosol observations from satellite can provide an independent measure of some key climate parameters in parallel with model predictions.

    One key measurement that satellites are able to provide is the direct shortwave radiative effect of aerosols at the top of the atmosphere. By aerosol direct shortwave radia-
²⁰ tive *effect* we mean the difference in shortwave radiative flux between having aerosols present and having no aerosols at all. This is different from aerosol shortwave direct radiative *forcing*, which is the radiative effect of anthropogenic aerosols only. Analysis suggests that by characterizing aerosol particle size from space, there is information available to the satellites to classify aerosol into natural and anthropogenic and there-
²⁵ fore to determine the anthropogenic portion of the aerosol loading and subsequently determine aerosol forcing from the aerosol effect (Kaufman et al., 2002; Kaufman et al., in review, 2005[1]). However, the focus of the present study is the straightforward

---

[1] Kaufman, Y. J., Remer, L. A., Tanré, D., Li, R.-R., Kleidman, R. G., Mattoo, S., Levy, R., Eck, T., Holben, B. N., Ichoku, C., Martins, J. V., and Koren, I.: A critical examination of the

Aerosol effect on solar radiation from MODIS

L. A. Remer and
Y. J. Kaufman

Title Page

Abstract   Introduction

Conclusions   References

Tables   Figures

◄   ►

◄   ►

Back   Close

Full Screen / Esc

Print Version

Interactive Discussion

EGU

estimate of aerosol total direct radiative effect.

In this study, we make global and regional estimates of the clear-sky aerosol short-wave radiative effect over the oceans using an internally consistent set of parameters from the MODIS aerosol retrieval. We first put the present study in context with other
measurement-based estimates of aerosol effect. We then describe the MODIS aerosol retrieval over ocean and the information available. The paper then describes the radiative transfer model, how we adapt the MODIS data to be used as inputs to the model, how we calculate the regional and global instantaneous and 24 h daily averages of the aerosol direct radiative effect. The results include estimates of monthly mean direct
aerosol radiative effect over the oceans, globally and in 13 regional sections, for both the Terra and Aqua satellites.

2. Background

There have been various approaches to using satellite data as the basis for determining aerosol direct radiative effect. One approach is to combine the satellite data with chemical transport model information (Yu et al., 2004). This method allows apportionment of radiative effects to chemical species, but requires assumption of aerosol optical properties. Another approach is to use MODIS to measure aerosol loading in the form of aerosol optical thickness and to use simultaneous observations of the radiation field by CERES (Christopher and Zhang, 2002; Zhang et al., 2005b). Using CERES eliminates the need to assume aerosol optical properties, but does require aerosol dependent angular distribution models (Loeb et al., 2003a, b; Zhang et al., 2005a). Furthermore, the large CERES footprint (20 km at nadir) biases results of clear sky direct radiative effects to situations dominated by large high pressure systems. Loeb and Manalo-Smith

residual cloud contamination and diurnal sampling effects on MODIS estimates of aerosol over ocean, IEEE Trans. Geosci. Remote Sens., in review, 2005.

L. A. Remer and
Y. J. Kaufman

(submitted, 2005) [2] avoid this cloud-free sky bias by basing their estimate on the finer resolution MODIS observations. They first determine the relationship between MODIS narrowband radiances and CERES broadband ones, and use the relationship to make a narrowband to broadband conversion.

5   In this study we present an alternative method using MODIS data alone to estimate direct aerosol radiative effect over the oceans. As mentioned above, the 500 m spatial resolution of MODIS observations reduces any unnatural bias to cloud-free conditions. Unlike the CERES studies, above, we use an offline radiative transfer model (Chou et al., 1992) to make the conversion between MODIS-measured narrowband angular

10 radiances and broadband hemispheric fluxes in one step. In this way we avoid the empirical model that translates CERES angular measurements to hemispheric flux. Unlike the other studies that use models we do not have to go looking for outside sources for information to use as input to the model. The MODIS aerosol retrieval provides a complete set of aerosol optical properties that best match the spectral radiance at the top

15 of atmosphere. A similar method maintaining consistency between retrieval and flux calculations was done using POLDER data (Boucher and Tanré, 2000). By matching the measured spectral radiance, the influence of errors in the MODIS assumptions on the derived flux are diminished. For example, both the flux and the radiance are proportional to first order to the single scattering albedo (ω_o). An error in the ω_o will

20 cause an error in the derived aerosol optical thickness (τ_a). However, if the derived τ_a is used with the same assumed ω_o to derive the flux, the errors in ω_o and τ_a will cancel, resulting in the correct value of derived flux, at least in the single scattering approximation.

---

[2]Loeb, N. G. and Manalo-Smith, N.: Top-of-Atmosphere direct radiative effect of aerosol over the global oceans from merged CERES and MODIS observations, submitted to J. Clim., 2005.

Title Page

Abstract | Introduction

Conclusions | References

Tables | Figures

◄◄ | ►►

◄ | ►

Back | Close

Full Screen / Esc

3. The MODIS aerosol retrieval over ocean

The MODIS satellite sensor has been observing and reporting on aerosol characteristics since the beginning of the Terra satellite mission in 2000 (Ichoku et al., 2002; Chu et al., 2002; Remer et al., 2002). MODIS measures radiance ($Wm^{-2}sr^{-1}$), denoted

5 as L, in 36 channels. Reflectance is calculated from these measurements according to the definition $\rho = \pi L/(\mu_o E_o)$ where μ_o is the cosine of the solar zenith angle and E_o is the extraterrestrial solar flux (Wm^{-2}) in the given spectral band. Of the 36 MODIS channels 6 channels (0.55–$2.13\,\mu m$) are directly used to retrieve aerosol information from scenes over ocean (Tanré et al., 1997; Remer et al., 2005). While MODIS spatial

10 resolution ranges from 250 m to 1000 m depending on wavelength, the 6 channels used in the aerosol algorithm are all at resolution of 250 or 500 m. The 250 m bands are degraded to 500 m, and thus the basic resolution of the MODIS aerosol retrieval input is uniformly 500 m. This broad spectral range, coupled with the 500 m spatial resolution in these bands, permits a unique view of aerosols that cannot be duplicated with

15 any other sensor. Because of the fine spatial resolution and specialized cloud mask (Martins et al., 2002; Gao et al., 2002; Brennan et al., 2005), MODIS retrieves aerosol properties closer to clouds than other satellites such as AVHRR with its 1 km resolution or especially CERES with its 20 km footprint. On the other hand, close proximity to clouds may introduce "cloud contamination" into the aerosol optical thickness retrieval.

20 Recent studies have begun to estimate the proportion of the retrieved aerosol optical thickness attributed to cloud effects (Kaufman et al., 2005[1]; Zhang et al., submitted, 2005 [3]).

The MODIS aerosol retrieval makes use of a LookUp Table (LUT) consisting of calculated upwelling radiances (or when normalized as above, solar reflectances) at top

25 of atmosphere for each of the six wavelengths for a rough ocean surface, a variety of geometries, aerosol amounts and aerosol models (Remer et al., 2005). There are

---

[3]Zhang, J., Reid, J. S., and Holben, B. N.: An analysis of potential cloud artifacts in MODIS aerosol optical thickness products, Geophys. Res. Lett., submitted, 2005.

EGU

L. A. Remer and
Y. J. Kaufman

9 aerosol models in the LUT. Four of the models represent submicron (fine) mode aerosol particles, and five of the models represent supermicron (coarse) mode particles. Each of the nine models consists of a monomodal lognormal size distribution, and real and imaginary refractive indices. Thus, a unique spectral dependence of extinction, single scattering albedo (ω_o) and assymetry parameter (g) is defined for each model.

In the retrieval process, the algorithm is looking for a combination of fine and coarse mode models to accurately represent the spectral reflectances measured by MODIS at the top of atmosphere. The modes from the LUT are combined using η as the weighting parameter,

$$\rho_\lambda^{\mathrm{LUT}}(\tau_a) = \eta\rho_\lambda^{\mathrm{f}}(\tau_a) + [1 - \eta]\rho_\lambda^{\mathrm{c}}(\tau_a) \, . \tag{1}$$

The inversion finds the pair of fine and coarse modes and the τ_a and η that minimizes the error (ε) defined as

$$\varepsilon = \sqrt{\frac{\sum_{\lambda=1}^{6} N_\lambda \left(\frac{\rho_\lambda^{\mathrm{m}} - \rho_\lambda^{\mathrm{LUT}}}{\rho_\lambda^{\mathrm{m}} + 0.01}\right)^2}{\sum_{\lambda=1}^{6} N_\lambda}} \, , \tag{2}$$

where N_λ is the number of pixels at wavelength λ, $\rho_\lambda^{\mathrm{m}}$ is the measured MODIS reflectance at the wavelength λ and $\rho_\lambda^{\mathrm{LUT}}$ is calculated from the combination of modes in the Look Up Table, defined by Eq. (1). The 0.01 prevents a division by zero for the longer wavelengths under clean conditions. Typically solutions are found with $\varepsilon < 3\%$ (Remer et al., 2005).

The solution represents the best fit of the LUT reflectances to the actual reflectances that MODIS measures. The combination of the two chosen modes, τ_a and η represent a derived aerosol model from which a variety of parameters including ω_o and g can be inferred. The combination of τ_a, ω_o and g represent the aerosol optical properties

that best fit the spectral reflectances at top of atmosphere. This is not saying that the MODIS algorithm is retrieving ω_o or g with any accuracy. There could be and are compensating errors associated with the retrieval of any one of the parameters. For this reason we do not make an attempt to estimate radiative effects at the surface,
which are particularly sensitive to the value of ω_o. However, the combination of MODIS retrieved τ_a, ω_o and g, when used consistently has to produce the best fit to the spectral reflectances at top of atmosphere.

4. Estimating aerosol radiative effect at top of atmosphere

4.1. The MODIS aerosol data

We will use the results of the MODIS aerosol retrieval as a consistent set of aerosol optical properties: τ_a, ω_o, and g, that will be input into a column radiative transfer climate model (Chou et al., 1992; Chou and Suarez, 1999) to calculate the upwelling hemispheric broadband fluxes at the top of atmosphere. The MODIS data we use are the Level 3 monthly mean aerosol optical thickness by model, reported at 0.55 μm on a 1-degree grid over oceans (King et al., 2003). This product gives us the monthly statistics based on the original 500 m resolution data. Over the course of a month, MODIS views the same 1-deg square with a wide variety of view angles. This works to reduce the uncertainty in calculating flux from the individual angular observations. The data from the Terra satellite form a time series from September 2001 to October 2002, and additionally from June 2003 to October 2004. The 7 months of data in 2002–2003 are missing due to a reprocessing of the data occurring during the time of this analysis. The data from the Aqua satellite form a continuous time series from October 2002 to November 2004.

The MODIS-derived aerosol optical thickness product has been compared extensively with AERONET observations (Holben et al., 1998). Comparisons are made both in terms of individual observations collocated in space and time (Ichoku et al., 2005;

Remer et al., 2005) and also comparisons of independently derived monthly mean values (Remer et al., 2005; Kleidman et al., submitted, 2005 [4]). These evaluations suggest that the MODIS aerosol optical thickness retrieval over oceans agrees with AERONET to within $\pm 0.03 \pm 0.05 \tau_a$. Even where the scatter from individual retrievals
5 exceeds expectations, the scatter is random, suggesting that long-term statistics may be even more accurate (Remer et al., 2005).

When MODIS data are collocated in time with AERONET data, MODIS benefits partially from AERONET's more aggressive cloud clearing algorithm. Thus, uncertainty may be larger and biases may exist in MODIS retrievals of aerosol optical thickness
10 that has not been previously reported in the validation studies. For example, MODIS may incorrectly make an observation and report an optical thickness for a scene with cloud contamination. AERONET would not make an observation in those conditions. Therefore, that contaminated MODIS retrieval would never make it to the validation scatter plots because there would be no corresponding AERONET point. Because
15 of these missing points, the reported uncertainty of $\pm 0.03 \pm 0.05 \tau_a$ may be overly optimistic, and MODIS retrievals could be biased high at all levels and scales. Recently this potential problem has been addressed and quantitatively estimated. We know that the cloud fraction, as measured by the MODIS satellite, is about 50% of its global values in the validation data sets used to collocate MODIS and AERONET. Also, recent analysis
20 of MODIS-derived thin cirrus reflectances and aerosol optical thickness retrievals suggests that roughly 0.01–0.02 of the MODIS aerosol optical thickness at 0.55 μm may be attributed to thin cirrus contamination and not aerosol at all (Kaufman et al., 2005[1]).

---

[4]Kleidman, R. G., O'Neill, N. T., Remer, L. A., Kaufman, Y. J., Eck, T. F., Tanré, D., Dubovik, O., and Holben, B. N.: Comparison of MODIS and AERONET remote sensing retrievals of aerosol fine mode fraction over ocean, J. Geophys. Res., submitted, 2005.

4.2. The Radiative Transfer Model

We use the radiative transfer model CLIRAD-SW (Chou et al., 1992; Chou and Suarez 1999) to calculate the hemispherical flux at the top of the atmosphere. CLIRAD-SW includes the absorption and/or scattering due to water vapor, various gases, aerosols clouds and the surface. Fluxes are integrated over the full solar spectrum, from $0.175 \, \mu$m to $10 \, \mu$m. The reflection and transmission of clouds and aerosol layers are calculated from the δ-Eddingtion approximation and the fluxes calculated using the two-stream adding approximation. Note that we use the model only in cloud free conditions.

CLIRAD-SW requires input of aerosol optical properties in 11 spectral bands, 7 in the ultraviolet, 1 in the 0.40–0.70 μm visible range, 1 in the near-infrared (0.70–1.22 μm), and 2 in the mid-infrared (1.22–10.0 μm). MODIS reports aerosol optical properties in 7 bands (0.47–2.13 μm), none in the ultraviolet. We translate the MODIS values to the wavelengths needed by the model by finding the wavelength of the solar-weighted MODIS extinction in each of CLIRAD-SW's bands,

$$\overline{\beta\text{ex}}(\overline{\lambda}, \text{mode}) = \sqrt{\frac{\int_{\lambda 1}^{\lambda 2} S(\lambda)\beta\text{ex}(\lambda, \text{mode})d\lambda}{\int_{\lambda 1}^{\lambda 2} S(\lambda)d\lambda}} \qquad (3)$$

with $S(\lambda)$ the solar spectrum (Neckel and Labs, 1981), $\beta\text{ex}(\lambda, \text{mode})$ the spectral extinction for each of the MODIS modes, and $\overline{\beta\text{ex}}(\overline{\beta}, \text{mode})$ the weighted value used for the CLIRAD-SW input for the band defined between $\lambda 1$ and $\lambda 2$. The representative wavelength is $\overline{\lambda}$, and the MODIS optical properties are interpolated or extrapolated to this value for each of the nine MODIS modes and each CLIRAD-SW band.

The interpolation/extrapolation of MODIS values to CLIRAD-SW bands introduces uncertainty in the final derivation of radiative effect. However, Ichoku et al. (2003) discuss that the final results of flux calculations, especially at top of the atmosphere are mostly insensitive to the extrapolation to the UV or mid-IR bands. The main sensitivity of translating input from the MODIS observations to the CLIRAD-SW bands is to the

Title Page

Abstract | Introduction

Conclusions | References

Tables | Figures

◀ | ▶|

◀ | ▶

Back | Close

Full Screen / Esc

Print Version

Interactive Discussion

EGU

interpolation in the only visible band, $\lambda = 0.40\,\mu m$ to $\lambda = 0.70\,\mu m$, corresponding closely to the MODIS primary channel ($0.55\,\mu m$), and making the interpolation more certain. The uncertainty in the final results from many sources of error is fully discussed in Sect. 6.

5   We set the ocean surface albedo to be 0.07, and use the midlatitude profiles for temperature and humidity for all model runs. The sensitivity tests in Ichoku et al. (2003) show that the results at top of atmosphere are insensitive to choice of atmospheric profile, but are sensitive to the choice of ocean albedo. A Δalbedo=0.01 will result in an uncertainty of radiative effect of ~2–4% depending on solar zenith angle

10   We run CLIRAD-SW separately for each of the 9 sets of aerosol optical properties corresponding to the 9 MODIS modes, for a range of aerosol optical thickness values and for 9 solar zenith angles. From the model output we subtract the net radiative flux at top of the atmosphere for no aerosol optical thickness ($\tau_a = 0$) from the values calculated at each of the other values of aerosol optical thickness. This becomes a

15   Look Up Table (LUT) of aerosol effect at the top of the atmosphere. An example of such results are displayed in Fig. 1 averaged over the 24-h period for a location at the equator at the equinox so that we are simulating a 12-h day with the solar zenith angle equal to 0 at noon. We see that for a specific τ_a, even for a moderate value such as 0.20, the effect at top of the atmosphere can vary by approximately $5\,\mathrm{Wm}^{-2}$, depending

20   on the type of aerosol present.

4.3.   The distribution of aerosol type

The MODIS Level 3 monthly mean statistics include the product, Optical_Depth_By_Models_Ocean, that provides the optical depth at wavelength $0.55\,\mu m$ attributed to each of the 9 modes in the MODIS algorithm. This product provides the

25   basis for determining the distribution of aerosol properties over the world's oceans. As an illustration we divide the global oceans into 13 sections defined in Fig. 2, and calculate the mean optical thickness attributed to each of the MODIS modes for every month. Examples of the distribution of τ_a among the different modes observed from

L. A. Remer and
Y. J. Kaufman

the Terra satellite for three such sections and one section from the Aqua satellite are shown in Fig. 3.

Section 9 is the cleanest of the 13 sections in terms of aerosol loading with an annual average τ_a=0.09. In this southern tropical Pacific section the primary mode chosen by MODIS is mode=7, and to a lesser extent mode=6, both corresponding to coarse marine sea salt aerosols. Fine modes 1 and 4 also make a contribution, especially in the non-summer months. The fine mode may represent dimethyl sulfide (DMS). There is almost no contribution from fine modes 2 and 3, or coarse modes 5, 8 and 9. This is how Terra-MODIS interprets the background marine aerosol, and Aqua-MODIS (not shown) is similar but with less coarse mode 6, slightly more in modes 1 and 9.

Section 6, off the coast of West Africa contains both transported Saharan dust and biomass burning smoke with an annual average τ_a=0.20. In contrast to Sect. 9, we see that in Terra Sect. 6 modes 8 and 9 make a contribution to the total aerosol optical thickness. These two modes correspond to mineral dust. In addition, mode 4 is much stronger than in the purely background aerosol of Sect. 9. The broad size distribution of mineral dust includes long tails into the submicron region that the MODIS retrieval interprets as optical thickness in the largest fine mode. The winter months tend to have a different distribution of modes than the rest of the year, possibly due to a greater contribution by biomass burning aerosol during that season. The Aqua Section 6 distribution (not shown) is similar to Terra, but with less contribution by mode 6, and more in the dust modes 8 and 9.

Section 4 is the region down stream from north and central Asia with an annual mean τ_a=0.20. In Terra-MODIS we see a broad distribution of aerosol modes, with the summer months exhibiting large increases in fine modes 2 and 3. MODIS interprets smoke and pollution particles mostly as an increase in modes 2 and 3. Although dust is prevalent in this region in the Spring months only a slight elevation in mode 8 is noted. The Aqua-MODIS representation in this section is quite different, showing very little optical thickness due to mode 6, much more optical thickness in the dust modes of 8 and 9, and very different distributions amongst the fine modes. Annual mean fine mode

fraction from Terra for Sect. 4 is 0.60, while for Aqua it is 0.70. Note that unlike annual mean values of fine mode fraction published in other studies these mean values were not weighted by τ_a and are used only to compare Terra and Aqua here. Differences between Terra and Aqua arise from a combination of basic calibration differences in the two instruments and also small changes to the MODIS aerosol retrieval algorithms that may be implemented at different times in the separate processing for Terra and Aqua. The MODIS retrieval of aerosol size and choice of aerosol model are especially sensitive to instrument calibration (Chu et al., 2005).

   The examples in Fig. 3 demonstrate two points. The first is that the global distribution of aerosol optical properties is more complex than simply the distribution of aerosol optical thickness, or even the distribution of fine mode fraction. The second point is that differences between Terra and Aqua demonstrate the sensitivity of the retrieval algorithm to small perturbations in instrument calibration and software.

4.4.   Deriving regional and global daily average aerosol radiative effect

To calculate the aerosol radiative effect we combine the distribution of aerosol modes from the MODIS retrieval (Fig. 3) with the calculated radiative effect as a function of mode (Fig. 1). The MODIS-measured aerosol optical thickness in each mode, τ_a (mode, lat, lon) and the solar zenith angle are used as indices in the radiative effect look-up table, $F[\tau_a(\text{mode, lat, lon}), \theta_o]$. Then we sum the results over all nine modes.

$$F(\text{lat, lon}) = \sum_{\text{mode}=1}^{9} f[\tau_a(\text{mode, lat, lon}), \theta_0] . \qquad (4)$$

This is the monthly mean aerosol effect at top of atmosphere for a particular 1-deg grid square, instantaneously at the time of satellite overpass.

   We estimate the 24-h daily average radiative effect from the instantaneous values calculated from the MODIS observations. To do so, we return to the CLIRAD-SW model and simulate the diurnal cycle in hourly increments of the aerosol effect for

7 latitudes and 12 months, assuming that the aerosol AOT and properties do not vary systematically through the day. We combine the results of the nine MODIS modes based on the annual mean global aerosol optical thickness and distribution over the nine modes. From this modeling effort we are able to calculate the daily average and

5 the ratio of the instantaneous at the time of satellite overpass to the daily average. The Terra overpass is considered to be 10:30 am, and the Aqua over pass 01:30 pm. An example of these ratios is shown in Fig. 4. Thus for any particular month,

$$F24(lat, lon) = F(lat, lon) \frac{F^{calc}24(lat, month)}{F^{calc}I(lat, month)} \qquad (5)$$

with F24(lat,lon) the 24-h daily average radiative effect for the grid square based on the

10 MODIS observations, F(lat,lon) the MODIS-derived instantaneous radiative effect from Eq. (4), $F^{calc}24$(lat,month) the model-derived daily average for month and latitude and $F^{calc}I$(lat,month) the model-derived value at the instantaneous time of overpass.

The ratios of $F^{calc}24$(lat, month)/$F^{calc}I$(lat, month) are dependent on aerosol optical thickness and type. There is a 10% uncertainty in F24(lat,lon) introduced by the ratios

15 due to uncertainty in aerosol type, based on testing the differences in final F24 between using fine mode 2 or coarse mode 7. There is an additional 8% uncertainty introduced by varying the mean τ_a used in the calculation from global mean values to $\pm\sigma$ one standard deviation from global mean values. Because of the symmetry around solar noon of the Terra and Aqua over pass times, the ratios are the same for both satellites.

20 The Level 3 monthly mean MODIS data that we use will report a monthly mean value in any grid square that has at least one retrieval in that square during the month. Because the basic resolution of the MODIS aerosol retrieval is 10 km, a grid square may have as many as 3000 retrievals in a 30 day month. Clouds, glint, geometry and orbital considerations reduce that number considerably. However, there does remain a

25 significant difference between a grid square with just one 10 km retrieval in the entire month and another square with several hundred retrievals. This difference would be minimal had we used daily data instead of monthly. In order to reconstruct the statistics

EGU

realized from daily data as we calculate regional and global means, we simply weight each monthly value by the number of MODIS aerosol observations for that month and grid square, Nobs(lat, lon). We also weight by cosine of the latitude to account for the decreasing surface area and corresponding decreasing contribution to the total global or regional radiative effect toward the poles.

$$F24(sect) = \sum_{lat} \sum_{lon} F24(lat, lon)Nobs(lat, lon)\cos(lat) \tag{6}$$

$$F24\_global = \sum_{lat} \sum_{lon} F24(lat, lon)Nobs(lat, lon)\cos(lat) \,, \tag{7}$$

where F24(sect) is the daily mean radiative effect at top of atmosphere for one of the 13 sections defined in Fig. 2 and F24_global is the global value. F24(sect) and F24_global are calculated for every month of available data.

5. Results

Figure 5 shows the 24-h MODIS-derived aerosol radiative effect from the Terra satellite at top of the atmosphere for four seasons, and Fig. 6 gives the numerical values for both the aerosol optical thickness and the radiative effect. The locations noted for high aerosol loading unsurprisingly also show prominent radiative effect from these aerosols. Such locations as the Atlantic coast of Africa (Swap et al., 2003; Tanré et al., 2003), the coasts of Asia (Huebert et al., 2003) and the northern midlatitudes in spring (Chin et al., 2004) all report radiative effect in excess of $-15\,\mathrm{Wm}^{-2}$. More surprising is the band of strong effect that occurs in the southern midlatitudes during Northern Fall and Winter.

Figure 7 shows time series of Terra-MODIS monthly mean aerosol optical thickness, τ_a, for each section and also the global value for both Terra and Aqua satellites. These τ_a are weighted by the number of retrievals in each grid box, analogous to Eqs. (6)

Aerosol effect on solar radiation from MODIS

L. A. Remer and
Y. J. Kaufman

and (7) for F(lat, lon). These weighted τ_a are biased low when compared to unweighted values, but better represent the clear-sky direct radiative effect, which is the subject of the present study. Annual mean values of the weighted τ_a over the global oceans for Terra-MODIS is 0.13, the unweighted value is ∼0.14. For Aqua-MODIS the weighted

5   and unweighted values are 0.12 and 0.13, respectively. The time series plots show a great amount of variation in optical thickness between sections, hemispheres and seasons. However the global mean value remains remarkably constant. The sections of highest aerosol optical thickness include the Asian outflow (Sect. 4), the Saharan outflow (Sect. 6) and the Arabian Sea (Sect. 7). Note that the cleanest region is the

10 south tropical Pacific, but that the midlatitude southern ocean also has relatively little aerosol loading, despite the strong radiative effect seen in Fig. 5.

The center row of Fig. 7 shows a time series of monthly mean aerosol radiative effect from Terra-MODIS for each section, F24(sect), and also F24_global for both Terra and Aqua. The same regional and seasonal variations are seen in the radiative effect as

15 in the optical thickness. The bottom row of Fig. 7 shows a time series for radiative efficiency in units of Wm^{-2} per unit $\tau_{a,}$ again from Terra-MODIS. Radiative efficiency is defined as the slope of the linear regression equation calculated from the relationship of F24 and τ_a. In this work it is not a simple ratio of F24/τ_a. There is much more variability in the radiative efficiency than in either τ_a or F24, not only regionally, but globally as

20 well. The higher the latitude the larger the solar zenith angle and the greater the radiative efficiency. Section 13, the midlatitude southern ocean, has a strong radiative efficiency, explaining the apparent contradiction between low aerosol optical thickness and relatively high F24.

Table 1 gives the annual mean global values of τ_a, F24_global and the radiative

25 efficiency for 5 complete calendar years, 2 from Terra and 3 from Aqua. The global mean value of F24 for Terra is approximately -5.6 ±0.3 Wm^{-2} and –5.9±0.3 Wm^{-2} for Aqua. The global mean value of aerosol efficiency is approximately –43 $Wm^{-2}\tau_a^{-1}$ for Terra and –48 $Wm^{-2}\tau_a^{-1}$ for Aqua.

The year to year variation of either platform is remarkably small. However, even

though the two platforms agree to within the given error bars, Aqua does report higher values. This is not due to a global diurnal variation of observed τ_a, because Aqua's value of τ_a is actually smaller than Terra's in this data set. The two platforms do report different distributions of aerosol over the 9 modes (Fig. 2), suggesting either different aerosol types at the two overpass times, or more likely, uncertainties in the two sensors' calibrations or properties that result in retrievals of different aerosol modes. For example, the 1.6 μm channel on Aqua is not functional and the aerosol retrieval is reduced to 5 channels of input. Retrieval of aerosol size parameters strongly depend on instrument calibration.

A more detailed comparison between Terra and Aqua is shown in Fig. 8. Here monthly sectional means derived from the two sensors are plotted against each other in scatter plots. Northern and southern hemispheres are plotted separately, with midlatitude separated from tropical sections by symbol. We use different scales on the axes in the two hemispheres. Aqua aerosol optical thickness (τ_a) is systematically lower than Terra's for all sections and seasons, north and south of the equator, both midlatitudes and tropics. However, Aqua's radiative effect (F24) is similar to Terra's in the midlatitudes, while systematically more negative in the tropics. The reason is the stronger efficiency (F24/gτ_a) observed by Aqua in all regions and seasons. The stronger efficiency compensates for the lower τ_a in the midlatitudes, but overcompensates in the tropics, causing the Aqua tropical F24 values to be more negative than Terra's. For these matching monthly-sectional mean values, Aqua τ_a are lower than Terra's by 8% in the midlatitudes and 3% in the tropics. The Aqua efficiencies are stronger by 6% in the midlatitudes and 15% in the tropics, while the Aqua radiative effect (F24) is 2% less negative than Terra's in the midlatitudes but 12% more negative in the tropics.

6. Random and systematic uncertainty

The uncertainties appearing in Table 1 are based on the following sources of unbiased uncertainty. The first source of error is the uncertainty of the MODIS radiances

themselves, ~2%. The second source of error is the initial MODIS retrieval of the sets of parameters, τ_a, ω_o and g, which match the observed spectral radiances to within 3% (Eq. (2)), and thus over an ensemble of measurements of various view angles encountered during a month of MODIS observations should also represent flux at top of atmosphere to within the same uncertainty. The third source of error arrives from initialization of the CLIRAD-SW model. Uncertainties in sea surface albedo of 0.01 will result in uncertainty of flux of ~3%, uncertainties in extrapolation of aerosol properties from MODIS wavelengths in the visible and near-infrared to the ultraviolet and mid-infrared introduce less than 1% error, while the choice of atmospheric profiles introduce negligible error. The last source of error arises from converting instantaneous radiative effect to 24-h daily averaged values. In making the conversion we model the diurnal cycle of radiative effect based on assuming global mean aerosol optical thickness and global mean distribution of aerosol type over the 9 MODIS modes. We determine uncertainty to these assumptions of aerosol properties from sensitivity studies that deviated aerosol type from one pure fine mode to one pure coarse mode, and then deviated aerosol amount one standard deviation from global mean values. The uncertainty to the conversion due to aerosol type adds a 10% error, while the uncertainty due to aerosol amounts introduces an 8% error. We take these errors originating in the conversion to 24-h averages to be random, although there could be systematic biases if assumptions underlying the original aerosol optical models are not realistic. Combining all these sources of uncertainty in a root mean square error sense results in an overall *random* uncertainty of 5.5% or roughly $0.3\,\mathrm{Wm}^{-2}$ for global values of $-5.5\,\mathrm{Wm}^{-2}$. The above error analysis assumes all uncertainties are random. Another source of uncertainty concerns the issue of residual cloud contamination in the retrievals, which introduce a biased error into the estimation of aerosol radiative effect. Cloud contamination will always increase aerosol optical thickness and therefore systematically introduce a high bias to our estimates of radiative effect. As discussed above in Sect. 4.1, we estimate the potential increase of optical thickness due to contamination may be as high as 0.015 to 0.020 optical thickness on a global basis (Kaufman et al., 2005[1];

Zhang et al., 2005[4]). Clouds will also modify the aerosol retrieval of the other two parameters of the solution set, creating their own signature in the calculated fluxes and estimates of radiative effect. It is unclear at this point, exactly how to interpret the effect of cloud contamination on the final results. However, if the global efficiencies in Table 1

5 remain the same with only the global mean aerosol optical thickness affected then as an approximation we can calculate a "cloud corrected" F24 by multiplying the Table 1 efficiencies by their respective global values of $(\tau_a - \Delta g \tau_a)$, where $\Delta \tau_a$ is the amount of optical thickness attributed to cloud contamination (0.015 to 0.020). For the first row of Table 1 $(\tau_a - \Delta \tau_a)$ is 0.11 to 0.115, which when multiplied by $-43.1 \, \mathrm{Wm}^{-2}$ per τ_a gives

10 us a range of corrected F24 to be -4.7 to $-5.0 \, \mathrm{Wm}^{-2}$. Applying the same calculation to the other years and satellites listed in Table 1 suggests that the Terra $-5.5 \, \mathrm{Wm}^{-2}$ and the Aqua $-5.9 \, \mathrm{Wm}^{-2}$ listed in the table should be taken as an upper bound of the estimate, and a cloud free number may be closer to -4.7 to $-5.2 \, \mathrm{Wm}^{-2}$.

7. Conclusions

15 We have estimated the regional and global value of total clear-sky aerosol shortwave radiative effect over the oceans in cloud free conditions to be $-5.5 \pm 0.3 \, \mathrm{Wm}^{-2}$ to $-5.9 \pm 0.3 \, \mathrm{Wm}^{-2}$ using an internally consistent set of MODIS retrieved aerosol parameters. Correcting for estimated cloud contamination, these numbers become $-4.7 \pm 0.3 \, \mathrm{Wm}^{-2}$ to $-5.2 \pm 0.3 \, \mathrm{Wm}^{-2}$ The global values of aerosol optical thickness and

20 radiative effect are remarkably consistent from season to season and year to year.

Individual regions show greater variability, spatially, seasonally and annually. For the most part, aerosol shortwave radiative effect is directly proportional to aerosol optical thickness, with the regions and seasons experiencing the highest optical thickness also experiencing the greatest radiative effect. However, because of the increased solar

25 zenith angle at higher latitudes, the midlatitude and polar regions have higher radiative efficiency and greater radiative effect for the same optical thickness found in the tropics. There are also differences in radiative efficiency due to different optical properties of

Aerosol effect on solar radiation from MODIS

L. A. Remer and
Y. J. Kaufman

aerosol in different regions.

There is a systematic bias between the results from the Terra and Aqua satellites with Terra showing 5% less effect and 11% weaker radiative efficiency than Aqua, despite its consistently higher values of optical thickness. Most of the differences between Terra and Aqua occur in the tropics. Note that the 5% difference is slightly smaller, not larger and in opposite direction than the difference in the AOT between the two satellites. This is the result of the compensation effects between errors made in the derivation of the AOT and in calculations of the aerosol radiative effect. In summary, the MODIS analysis of the aerosol effect on the radiative fluxes adds a new measurement perspective to a climate change problem dominated so far by models.

References

Boucher, O. and Tanré, D.: Estimation of the aerosol perturbation to the Earth's radiative budget over oceans using POLDER satellite aerosol retrievals, Geophys. Res. Lett., 27(8), 1103–1106, 2000.

Brennan, J. I., Kaufman, Y. J., Koren, I., and Li, R.-R.: Aerosol-cloud interaction – misclassification of MODIS in heavy aerosol, IEEE Trans. Geosci. Remote Sens., 43(4), 911–915, 2005.

Chin, M., Chu, D., Levy, R., Remer, L., Kaufman, Y., Holben, B., Eck, T., Ginoux, P., and Gao, Q.: Aerosol distribution in the northern hemisphere during ACE-Asia: Results from global model, satellite observations and sunphotometer measurements, J. Geophys. Res., 109, D23S90, doi:10.1029/2004JD004829, 2004.

Chou, M.-D.: A solar-radiation model for use in climate studies, J. Atmos. Sci., 50(5), 673–690, 1992.

Chou, M.-D. and Suarez, M. J.: A solar radiation parameterization (CLIRAD-SW) for atmospheric studies, NASA/TM-1999-104606, 15, 48, 1999.

Christopher, S. A. and Zhang, J.: Shortwave aerosol radiative forcing from MODIS and CERES observations over the oceans, Geophys. Res. Lett., 29(18), 1859, doi:1810.1029/2002GL014803, 2002.

Chu, D. A., Kaufman, Y. J., Ichoku, C., Remer, L. A., Tanré, D., and Holben, B. N.:

Validation of MODIS aerosol optical depth retrieval over land, Geophys. Res. Lett., 29, doi:10.1029/2001GL013205, 2002.

Chu, D. A., Remer, L. A., Kaufman, Y. J., and Schmidt, B.: Characterization of aerosol properties by MODIS during ACE-Asia Experiment, J. Geophys. Res., 110(D7), doi:10.1029/2004JD005208, 2005.

Gao, B.-C., Kaufman, Y. J., Tanré, D. and Li, R.-R.: Distinguishing tropospheric aerosols from thin cirrus clouds for improved aerosol retrievals using the ratio of 1.38-μm and 1.24-μm channels, Geophys. Res. Lett., 29, 1890, doi:1810.1029/2002GL015475, 2002.

Holben, B. N., Eck, T. F., Slutsker, I., Tanré, D., Buis, J. P., Setzer, A., Vermote, E., Reagan, J. A., Kaufman, Y. J., Nakajima, T., Lavenu, F., Jankowiak, I. and Smirnov, A.: AERONET– A federated instrument network and data archive for aerosol characterization, Rem. Sens. Environ., 66, 1–16, 1998.

Huebert, B. J., Bates, T. S., Russell, P. B., Shi, G. Y., Kim, Y. J., Kawamura, K., Carmichael, G., and Nakajima, T.: An overview of ACE-Asia: Strategies for quantifying the relation- ship between Asian aerosols and their climatic impacts, J. Geophys. Res., 108(D23), 8633, doi:8610.1029/2003JD003550, 2003.

Ichoku, C., Chu, D. A., Mattoo, S., Kaufman, Y. J., Remer, L. A., Tanré, D., Slutsker, I., and Hol- ben, B. N.: A spatio-temporal approach for global validation and analysis of MODIS aerosol products, Geophys. Res. Lett., 29, doi:10.1029/2001GL013206, 2002.

Ichoku, C., Remer, L. A., Kaufman, Y. J., Levy, R., Chu, D. A., Tanré, D., and Holben, B. N.: MODIS observation of aerosols and estimation of aerosol radiative forcing over southern Africa during SAFARI 2000, J. Geophys. Res., 108, doi:10.1029/2002JD002366, 2003.

Ichoku, C., Remer, L. A. and Eck, T. F.: Quantitative evaluation and intercomparison of morning and afternoon MODIS aerosol measurements from the Terra and Aqua satellites, J. Geophys. Res., 110, D10S03, doi:10.1029/2004JD004987, 2005.

Intergovernmental Panel on Climate Change (IPCC): Climate Change 2001 – The Scientific Basis, Cambridge Univ. Press, Cambridge, 2001.

King, M. D., Menzel, W. P., Kaufman, Y. J., Tanré, D., Gao, B.-C., Platnick, S., Ackerman, S. A., Remer, L. A., Pincus, R., and Hubanks, P. A.: Cloud and aerosol properties, precipitable water, and profiles of temperature and humidity from MODIS, IEEE Trans. Geosci. Remote Sens., 41, 442–458, 2003.

Loeb, N. G., Manalo-Smith, N., Kato, S., Miller, W. F., Gupta, S. K., Minnis. P., and Wielicki, B. A.: Angular distribution models for top-of-atmosphere radiative flux estimation from the

Aerosol effect on solar radiation from MODIS

L. A. Remer and
Y. J. Kaufman

Title Page

Abstract | Introduction

Conclusions | References

Tables | Figures

◄ | ►

◄ | ►

Back | Close

Full Screen / Esc

Print Version

Interactive Discussion

EGU

clouds and the Earth's Radiant Energy System instrument on the Tropical Rainfall Measuring Mission satellite, Part I: Methodology, J. Appl. Meteor., 42(2), 240–265, 2003.

Loeb, N. G., Loukachine, K., Manalo-Smith, N., Wielicki, B. A., and Young, D. F.: Angular distribution models for top-of-atmosphere radiative flux estimation from the clouds and the Earth's Radiant Energy System instrument on the Tropical Rainfall Measuring Mission satellite, Part II: Validation, J. Appl. Meteor., 42(12), 1748–1769, 2003.

Martins, J. V., Tanré, D., Remer, L. A., Kaufman, Y. J., Mattoo, S., and Levy, R.: MODIS Cloud screening for remote sensing of aerosol over oceans using spatial variability, Geophys. Res. Lett., 29, doi:10.1029/2001GL013252, 2002.

Neckel, H. and Labs, D.: Improved data of solar spectral irradiance from 0.33 to 1.25, Solar Physics, 74, 231–249, 1981.

Remer, L. A., Tanré, D., Kaufman, Y. J., Ichoku, C., Mattoo, S., Levy, R., Chu, D. A., Holben, B. N., Dubovik, O., Smirnov, A., Martins, J. V., Li, R.-R. and Ahmad, Z.: Validation of MODIS aerosol retrieval over ocean, Geophys. Res. Lett., 29, doi:10.1029/2001GL013204, 2002.

Remer, L. A., Kaufman, Y. J., Tanré, D., Mattoo, S., Chu, D. A., Martins, J. V., Li, R.-R., Ichoku, C., Levy, R. C., Kleidman, R. G., Eck, T. F., Vermote, E., and Holben, B. N.: The MODIS aerosol algorithm, products and validation, J. Atmos. Sci., 62(4), 947–973, 2005.

Swap, R. J., Annegarn, H. J., Suttles, J. T., King, M. D., Platnick, S., Privette, J. L., and Scholes, R. J.: Africa burning: A thematic analysis of the Southern African Regional Science Initiative (SAFARI 2000), J. Geophys. Res., 108, 8465, doi:8410.1029/2003JD003747, 2003.

Tanré, D., Kaufman, Y. J., Herman, M., and Mattoo, S.: Remote sensing of aerosol properties over oceans using the MODIS/EOS spectral radiances, J. Geophys. Res., 102, 16971–16988, 1997.

Tanré, D., Haywood, J., Pelon, J., Leon, J. F., Chatenet, B., Formenti, P., Francis, P., Goloub, P., Highwood, E. J. and Myhre, G.: Measurement and modeling of the Saharan dust radiative impact: Overview of the Saharan Dust Experiment (SHADE), J. Geophys. Res., 108(D8), 8574, doi:8510.1029/2002JD003273, 2003.

Yu, H., Dickinson, R. E., Chin, M., Kaufman, Y. J., Zhou, M., Zhou, L., Tian, Y., Dubovik, O., and Holben, B. N.: Direct radiative effect of aerosols as determined from a combination of MODIS retrievals and GOCART simulations, J. Geophys. Res., 109, doi:10.1029/2003JD03206, 2004.

Zhang, J., Christopher, S. A., Remer, L. A., and Kaufman, Y.: Shortwave aerosol radiative forcing over cloud-free oceans from Terra: 1. Angular models for aerosols, J. Geophys. Res.,

Aerosol effect on solar radiation from MODIS

L. A. Remer and
Y. J. Kaufman

Title Page

Abstract | Introduction

Conclusions | References

Tables | Figures

◄ | ►►

◄ | ►

Back | Close

Full Screen / Esc

Print Version

Interactive Discussion

EGU

110, D10S23, doi:10.1029/2004JD005008, 2005a.

Zhang, J., Christopher, S. A., Remer, L. A., and Kaufman, Y. J.: Shortwave aerosol radiative forcing over cloud-free oceans from Terra: 2. Seasonal and global distributions, J. Geophys. Res., 110, D10S24, doi:10.1029/2004JD005009, 2005b.

Aerosol effect on solar radiation from MODIS

L. A. Remer and
Y. J. Kaufman

EGU

L. A. Remer and
Y. J. Kaufman

Table 1. Annual global mean aerosol optical thickness (τ_a), radiative effect at top of atmosphere (F24_global) and radiative efficiency (F24/τ_a) observed from Terra- and Aqua-MODIS during various calendar years.

year	τ_a	F24_global (Wm^{-2})	F24/τ_a (Wm$^{-2}\tau_a^{-1}$)	F24 corrected for clouds
Terra Sep. 2001 to Aug. 2002	0.130	−5.5±0.3	−43.1	−4.7 to −5.0
Terra Sep. 2003 to Aug. 2004	0.129	−5.6±0.3	−43.8	−4.8 to −5.0
Aqua Sep. 2003 to Aug. 2004	0.122	−5.8±0.3	−47.8	−4.9 to 5.1
Aqua Dec. 2002 to Nov. 2003	0.123	−5.9±0.3	−48.3	−5.0 to 5.2
Aqua Dec. 2003 to Nov. 2004	0.123	−5.9±0.3	−48.1	−5.0 to 5.2

F24 corrected for clouds is an approximation based on estimates of cloud contamination in the aerosol optical thickness product of 0.015 to 0.020 on a global basis, over the oceans. Discussion in Sect. 6.

Title Page

Abstract   Introduction

Conclusions   References

Tables   Figures

◄   ►►

◄   ►

Back   Close

Full Screen / Esc

Print Version

Interactive Discussion

EGU
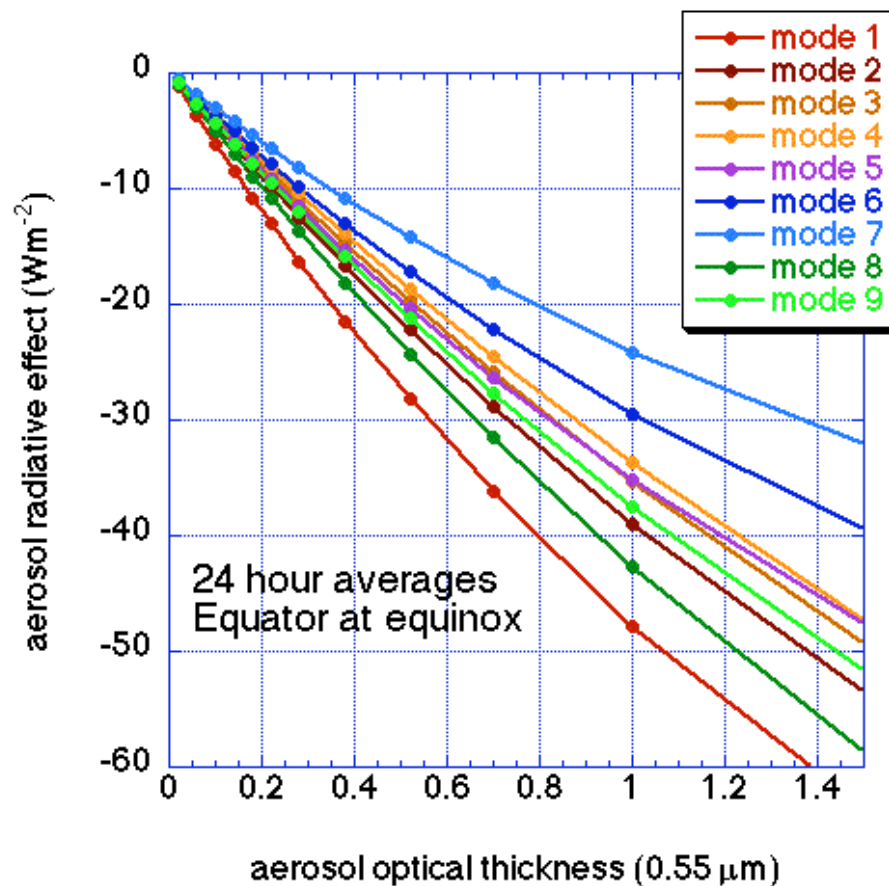
Fig. 1. Daily averaged aerosol radiative effect for a 12 hour day with the solar zenith angle equal to 0 at noon, a variety of aerosol optical thicknesses and the nine modes of the MODIS aerosol retrieval over ocean.

AOT L3 2004.JJA

Aerosol optical thickness (0.55 μm)
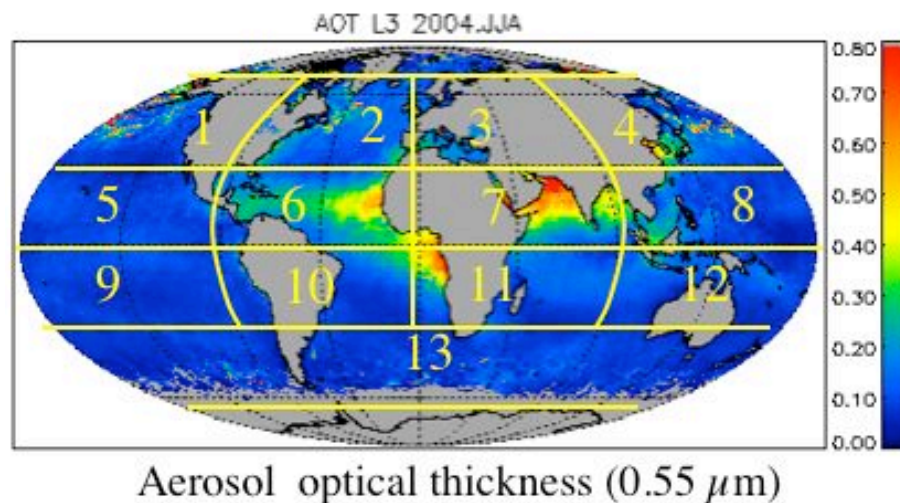
Fig. 2. Terra-MODIS observed seasonal mean aerosol optical thickness over oceans at 0.55 μm for the months June–July–August 2004. The 13 regional sections are also identified.

[EGU](#)
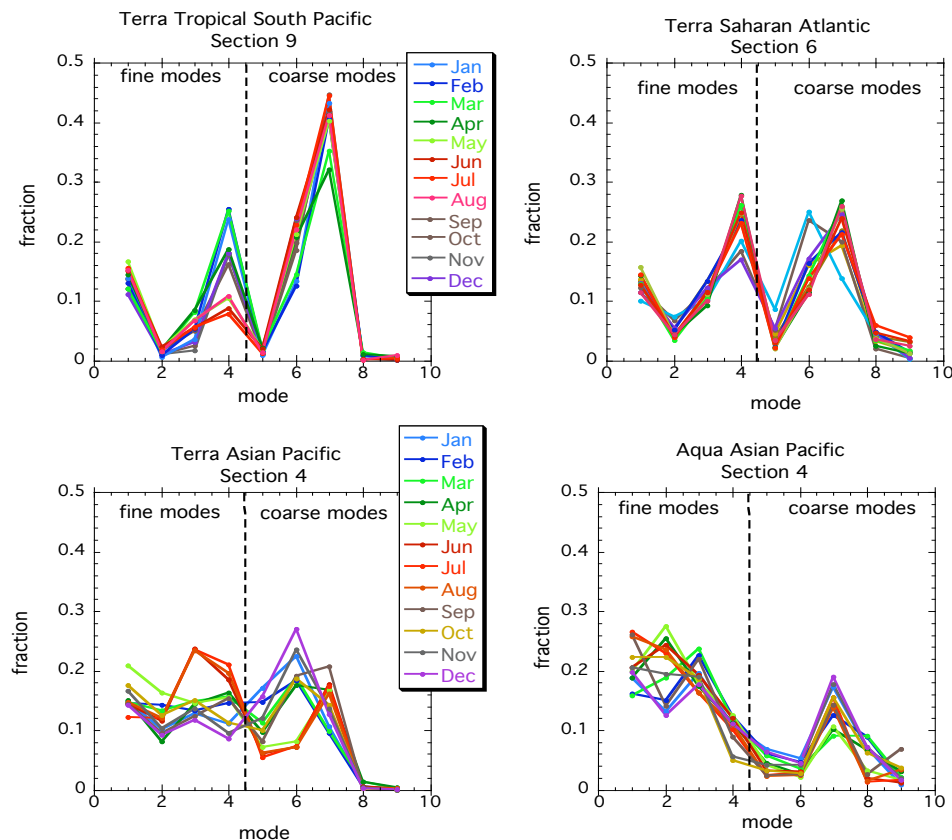
Fig. 3. Fraction of aerosol optical thickness attributed to each of the 9 MODIS modes for four example sections of Fig. 2 as functions of month. Months are composites of all available years of data. Three of the panels show distribution of mode optical thickness observed from the Terra satellite and the last panel (bottom right) shows observations from the Aqua satellite.

Title Page

Abstract	Introduction
Conclusions	References
Tables	Figures

|◄ | ►|
◄ | ►

Back | Close

Full Screen / Esc

Print Version

Interactive Discussion

EGU
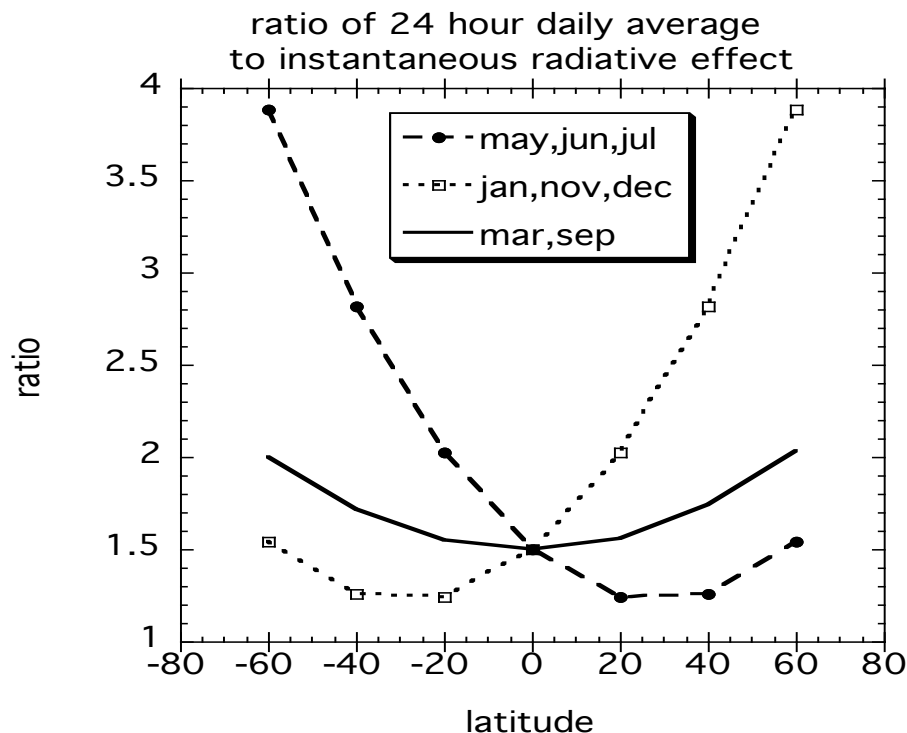
Fig. 4. Ratio of 24-h daily average radiative effect ($F^{calc}24$) to instantaneous radiative effect ($F^{calc}I$) as a function of latitude and month. Shown are selected months. The same ratio applies for Terra and Aqua.

EGU
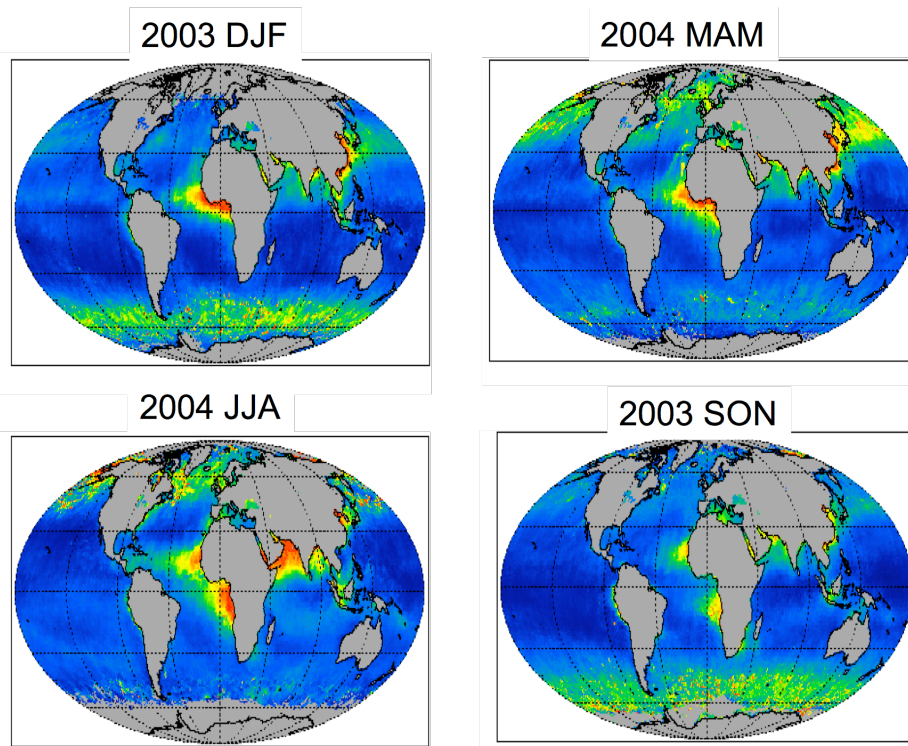
Fig. 5. Global distribution of MODIS-observed aerosol radiative effect at top of atmosphere from the Terra satellite for four seasons: Northern Winter 2003–2004 (upper left), Spring 2004 (upper right), Summer 2004 (lower left) and Fall 2003 (lower right).
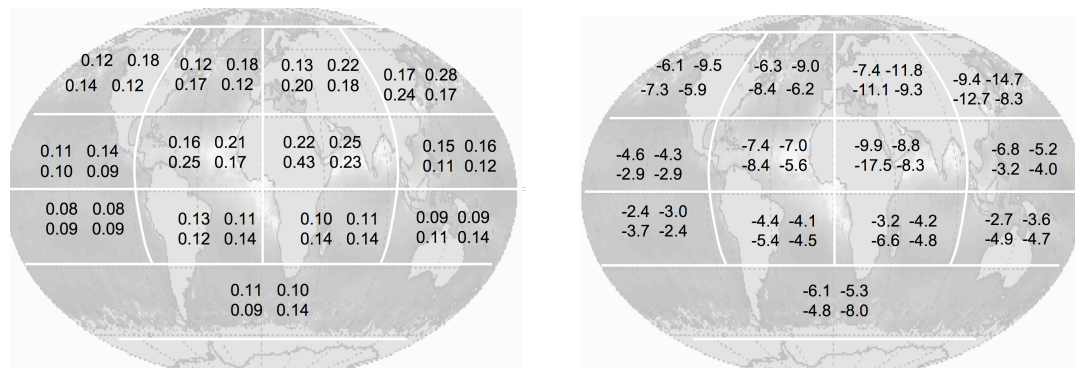
Fig. 6. Seasonal values of aerosol optical thickness (left) and aerosol radiative effect at the top of the atmosphere (right) from the Terra satellite. The four numbers in each latitude-longitude section represents a seasonal mean for that section from all available monthly data. Starting from the upper left corner and proceeding clockwise the seasons are Northern Winter, Spring, Summer and Fall, respectively. Radiative effect values of the bottom panel are fluxes in units of Wm^{-2}.

Fig. 7. Time series of monthly mean aerosol optical thickness (top row), radiative effect (center row), and radiative efficiency (bottom row) from Terra-MODIS for each of the 13 sections defined in Fig. 2 (dots). Also shown are the global mean values from both Terra (black line) and Aqua (blue line). The left panels show the northern midlatitudes, the center panels the northern tropics and the right panels the southern hemisphere. Terra is missing 7 months of data (2002–2003) due to data unavailability during reprocessing.
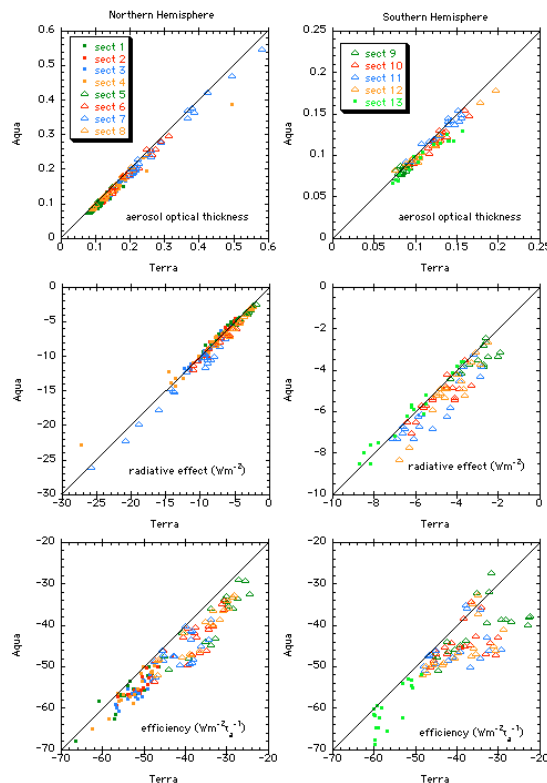
Fig. 8. Scatter plots of quantities derived from Aqua data plotted against those derived from Terra data. Each point is a monthly-sectional mean from each of the 13 sections whenever both satellites reported values. The quantities shown are aerosol optical thickness-τ_a (top), radiative effect – F24 (center) and radiative efficiency – F24/τ_a (bottom). The left column is for the Northern Hemisphere and the right column shows southern hemisphere results. Midlatitudes in both hemispheres are denoted by dots. Tropical sections in both hemispheres are denoted by open triangles.